4

Methods for Nonlinear Intersubject Registration in Neuroscience

Daniel Schwarz and Tomáš Kašpárek
Masaryk University
Czech Republic

1. Introduction

The human body is an amazingly complex system. Acquiring data about its static and dynamic properties yields massive amounts of information. The use of images is the most effective way to manage, present and interpret the vast quantities of that information in the clinical medicine and in the supporting biomedical research. Computational neuroanatomy is a new growing field of powerful applications in neuroscience. It promises an automated methodology to characterize neuroanatomical configuration of structural magnetic resonance imaging (MRI) brain scans. One of the crucial techniques in this methodology is image registration. It performs the task of spatial normalization of images according to a common reference anatomy termed as a brain atlas. It allows interpreting results of an image analysis in a standard anatomical coordinate system. Further, an atlas of brain makes it possible to find out how different is a subject brain compared with the common reference anatomy which represents certain population. Many approaches to registration of brain images assume same or functionally dependent intensities in the images across subjects. Thus, they allow the registration process to be driven by differences in intensities. They however do not count on intensity variations caused by various imaging conditions or tissue atrophy and degradation induced by neurological diseases. On the other hand, the image registration methods which are robust to such intensity variations enable only low-dimensional parametric transformations, which make it impossible to detect localized image differences without additional efforts. This chapter mainly contributes to the field of registration with the use of nonlinear locally adaptive transformations. Particularly, problems connected to matching brain image data obtained from various subjects and with various imaging conditions are solved here. Difficulties lie in the complex brain structure which varies widely from one individual to another. Other difficulties lie in the complex and unknown relations between intensities in images to be registered. A solution of a specific clinical task from the field of computational neuroanatomy is further presented.

Magnetic resonance imaging (MRI) is a highly successful diagnostic imaging modality, largely due to its rich set of contrast mechanisms. The signal intensity is a multivariable function, depending on many parameters. Partial listing includes proton spin density PD, spin lattice relaxation time T1, spin spin relaxation time T2, proton flow and diffusion. Due to its exceptionally high soft tissue contrast, MRI lends itself well to morphometric studies in the brain where clear distinction between structures is required (Ali et al., 2005).

1.1 Image registration in computational neuroanatomy

Recently the importance of new methods for image analysis has been growing due to the rapid development of medical imaging modalities. In the field of computational neuroanatomy, automated whole-brain methods for morphometry are utilized intensively for structural MRI brain volumetry besides the gold standard methods based on regions of interest (ROI) in the last decade. The automated whole-brain methods are voxel-based (VBM – voxel-based morphometry) or deformation-based (DBM – deformation-based morphometry). While the ROI-based methods need manual segmentation, which is time-consuming and subjective, the whole-brain methods use semi-automated or automated processing of images including their segmentation. Detection of pathological changes with the use of this type of methods is not limited by arbitrarily predefined borders. This fact is advantageous in disorders with progression of morphological changes during its duration.

Spatial normalization is a necessary step, which reduces an impact of individual variability in brain shape on the resulting assessment of its local characteristics. Spatial normalization of images in the stereotaxic space (Ashburner & Friston, 2000; Mechelli et al., 2005) with the use of deformable image registration is a common kernel of both VBM and DBM. In the VBM case, the registration suppresses only global shape differences, whereas DBM needs an image registration method, which covers complex anatomical variability including subtle local changes (Gaser C. et al. 2001; 2004). The endpoint of any morphometry method in computational neuroanatomy is usually a statistical parametric map which locates regions of significant anatomical differences between two groups of subjects. The map is a result of a standard parametric significance tests performed independently at each point of scalar fields or vector fields which describe the differences among the subject's anatomies.

An ongoing development of the morphomery methods lies in new designs for deformable registration methods (Ashburner, 2007; Schwarz et al. 2007) and in extending and refining the statistical apparatus which is used for computing statistical parametric maps destined for anatomical abnormality detection (Friston et al., 2007; Xu et al. 2008).

2. Registration of medical images

Image registration is a process of estimating a spatial transformation which maps each point of an image onto its corresponding point of another image (Rohr, 2001). Image registration is a fundamental problem in medical image analysis. A universal method does not exist due to the diversity of registration tasks. There are various approaches to the classification of image registration methods in surveys (Maintz & Viergever, 1998; Rohr, 2001; Zitova & Flusser, 2003; Gholipour et al, 2007).

2.1 Optimal registration

Optimal registration can be defined as an optimization problem with the goal of finding the spatial mapping that will bring the floating image N into alignment with the reference image M. Fig. 1 shows its basic steps.

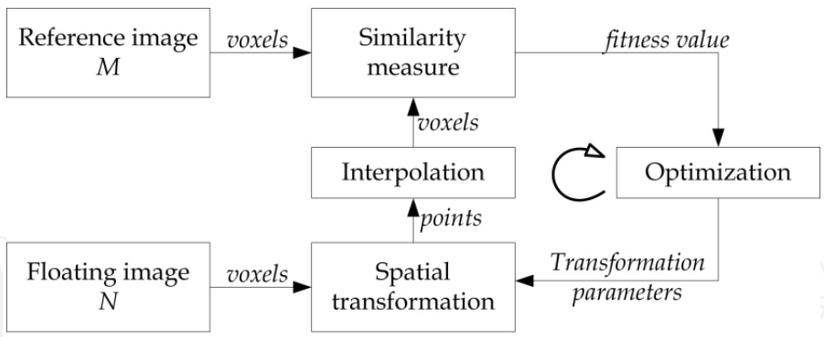

Fig. 1. Basic components of an optimal registration framework (Ibanez et al., 2003).

The spatial transformation φ_a^{-1} maps points from the reference image space to points in the floating image space. It is parameterized by a vector of parameters **a**. It is in fact an inverse mapping which is preferable as it avoids problems of holes with the forward mapping. The transformation is directly connected to interpolation which serves for evaluation of floating image intensities at non-grid positions. The similarity measure $S(M, N \circ \varphi_{\mathbf{a}})$ or its negative forms a criterion of optimality – a cost function which is minimized in the optimization over the search space defined by parameters of the spatial transformation.

The affine transformation is one of the most popular transformations used in image registration. It can be described by a single 4 × 4 matrix computed as a product of matrices representing translation, rotation, shearing and scaling.

The choice of an appropriate similarity measure is determined by the character of intensities in the floating and the reference image. Popular choices are based on intensity, correlation and mutual information. Supposing the image intensities to be discrete random variables, their mutual information (MI) is defined as (Ibanez et al., 2003):

$$I(M,N) = H(M) + H(N) - H(M,N) = \tag{1}$$
$$= \sum_{m,n} p_{MN}(m,n) \log_2 \frac{p_{MN}(m,n)}{p_M(m) p_N(n)},$$

where $I(M,N)$ is the mutual information of random variables M and N, $H(M)$ and $H(N)$ are entropies of M and N respectively and $H(M,N)$ is the joint entropy of M and N. It is rewritten to a form containing marginal probability density functions (PDF) $p_M(m)$, $p_N(n)$ and joint PDF $p_{MN}(m,n)$. MI gives a measure of the strength of the dependence between the random variables. The major advantage of using MI is that the actual form of the dependency does not have to be specified. Therefore, MI is well suited as a criterion of multimodal registration. The marginal and joint PDFs are estimated from image data by Parzen windowing (Viola, 1995; Studholme et al., 1999; Modersitzki, 2004) or by normalizing the joint histogram (Maes, 1998; Maintz et al., 1998).

An optimization technique is needed to find the spatial transformation defined by a vector of transformation parameters $\mathbf{a}=[a_1, ..., a_D]$. The number of parameters D ranges from six, for rigid body transformation, to twelve, for general affine transformation. In the case of deformable registration techniques, there are hundreds or even thousands of parameters. Optimization methods with no gradient computation requirement are typical for

correlation-based and mutual information based criterions. Powell's directions set method (Maintz et al., 1998; Pluim et al., 2001), downhill simplex method (Collins et al., 1994) and simulated annealing (Čapek et al., 2001; Kubečka & Jan, 2004) are most often examples.
To alleviate the problems associated with direct intensity interpolation methods, partial volume interpolation was proposed in (Maes, 1998) for mutual information based registration. It was further extended to a scheme called generalized partial volume (GPV) joint histogram estimation (Chen & Varshney, 2003).

2.2 Deformable registration

In many medical imaging applications, the global linear alignment does not provide a sufficient solution. A nonlinear transformation is necessary to correct the local differences in the images. Here, the process of finding such a transformation is termed as deformable registration. The reference image M and a floating image N are expected to be aligned by the global rigid body or affine transformation. The central idea behind deformable registration is to find local forces which will deform the floating image to make it more similar to the reference image, see Fig. 2. The transformation $\varphi(\mathbf{x})$ is usually split into the trivial identity part and a so called displacement field $\mathbf{u}(\mathbf{x})$ (Modersitzki, 2004):

$$\varphi(\mathbf{x}) = \mathbf{x} + \mathbf{u}(\mathbf{x}). \tag{2}$$

Computation of the displacement field involves local forces together with regularization provided by a spatial deformation model. Regularized mapping function ensures realistic registration results without tearing or folding of the image.

2.2.1 Parametric deformable registration

Parametric transformation (sometimes termed as low-dimensional) can be expanded in terms of some parameters a_i and basis functions ψ_i. The registration task is to determine the parameters of the transformation. Methods based on radial basis function (RBF) interpolation are used widely. Wendland's functions (Fornefett et al., 2001) and thin-plate splines (Kostelec et al., 1998; Pauchard et al., 2004) are examples of RBFs used in image registration. Other functions used for parametric deformations are B-splines (Rueckert et al., 1999; Rohlfing et al., 2003; Schnabel et al., 2003), components of discrete cosine transform (Ashburner & Friston, 2000) or wavelet basis functions (Downie & Silverman, 2001).
In the case of image deformation with the use of RBFs, the displacement field $\mathbf{u}(\mathbf{x})$ is controlled by a finite number of movable control points. The interpolation problem is solved separately for each coordinate of the displacement field:

$$u_k(\mathbf{x}): \mathbb{R}^d \to \mathbb{R}, \quad u_k(\mathbf{p}_i) = f_{i,k}, \quad i = 1...n, \quad k = 1...d. \tag{3}$$

where d is the image dimension, $\mathbf{p}_i$ constitute a given set of n control points and $\mathbf{f}_i$ are their translations. Using RBFs, the interpolant is constructed:

$$u_k(\mathbf{x}) = \sum_{j=1}^{m} b_j \phi_j(\mathbf{x}) + \sum_{i=1}^{n} a_i \psi\left(\left\|\mathbf{x} - \mathbf{p}_i\right\|\right), \tag{4}$$

where the first term is a linear combination of polynomials and the second term is a linear combination of RBFs. Here, ϕ_j are m polynomial components, ψ denotes a RBF and $\|\mathbf{x}\text{-}\mathbf{p}_i\|$ is the Euclidean distance from $\mathbf{x}$ to $\mathbf{p}_i$ and a_i, b_i are coefficients. A RBF is a function depending only on the distance from the origin: $\psi(\|\mathbf{x}\text{-}\mathbf{p}_i\|)= \psi(\mathbf{r})$. By inserting (4) into (3) and using constraints that guarantee polynomial precision (Amidror, 2002), a following system of linear equations for the coefficients $\mathbf{a}=[a_1, ..., a_n]^T$ and $\mathbf{b}=[b_1, ..., b_m]^T$ is obtained:

$$\begin{pmatrix} \mathbf{K} & \mathbf{P} \\ \mathbf{P}^T & 0 \end{pmatrix} \begin{pmatrix} \mathbf{a} \\ \mathbf{b} \end{pmatrix} = \begin{pmatrix} \mathbf{f}_k \\ 0 \end{pmatrix}, \tag{5}$$

where $\mathbf{K}$ is a $n \times n$ sub-matrix given by $K_{ij}=\psi(\|\mathbf{p}_i\text{-}\mathbf{p}_j\|)$, P is a $n \times m$ sub-matrix given by $P_{ij}=\phi_j(\mathbf{p}_i)$ and $\mathbf{f}_k=[f_{k,1}, ..., f_{k,n}]^T$ is a vector of the k^{th} coordinate of the control points' translations $\mathbf{f}_i$. The polynomial sub-matrix $\mathbf{P}$ depends on the type of RBF. For thin plate splines, it has its i^{th} row of the form $[1, x_{pi}, y_{pi}, z_{pi}]$, which are x, y and z-components of $\mathbf{p}_i$ (Donato & Belongie, 2002). Hence, there is a global influence of a control point on the resulting displacement field $\mathbf{u}(\mathbf{x})$. Compactly supported RBFs are another recent choice. Due to their positive definiteness, the regularity of the matrix $\mathbf{K}$ is ensured. Therefore, no polynomial part is needed and (5) reduces to:

$$\mathbf{K}\,\mathbf{a} = \mathbf{f}_k\,. \tag{6}$$

One of Wendland's functions (Wendland, 1995) is proposed for deformable image registration in (Fornefett et al., 2001):

$$\psi_{CP}(r) = (1-r)_+^4(4r+1). \tag{7}$$

Its mathematical properties hold for various spatial supports s, such that: $\psi_{CP}(r;s)= \psi_{CP}(\mathbf{r}/s)$. Compared to other RBFs, the use of compactly supported RBFs is highly efficient, as the matrix $\mathbf{K}$ is rather sparse and no transcendental functions are involved in the calculation. The support length s cannot be set arbitrary, as there is a fundamental condition of topology preservation. This requirement is satisfied if the determinant of the Jacobian of the deformation is non-negative.

2.2.2 Non-parametric deformable registration

Non-parametric deformable registration methods (sometimes termed as high dimensional) directly compute a displacement in every point most often by imitating real world transformations of deformable materials. One of the first proposed methods based on continuum mechanics was elastic matching (Ferrant et al., 2001; Alterovitz et al., 2004; Modersitzki, 2004). Only small deformations are assumed, thus linear elastic model can be used. In (Christensen et al., 1996), a viscous fluid model is used to control the deformation. The floating image is modelled as a thick fluid that flows out to match the reference image under the control of the local forces. Convolution filter methods for solving associated PDE were proposed in (Gramkow & Bro-Nielsen, 1997). A considerable piece of work is presented in (Rogelj et al., 2003; Rogelj & Kovačič, 2004), where Gaussian filters are used for

modelling the spatial deformation. The Gaussian filters are used to approximate the elastic as well as the fluid model. It is also successfully used for a so-called incremental model, which is used for image registration in (Peckar et al., 1998). A spatial deformation model made up from the elastic and the incremental model is proposed, in order to combine their advantages and thus improve the registration. The model consists of two convolution filters (Rogelj & Kovačič, 2004):

$$\mathbf{u}_f = k\mathbf{f}, \tag{8}$$

$$\mathbf{u}^i = \left(\mathbf{u}^{i-1} + \mathbf{u}_f * \mathbf{G}_I\right) * \mathbf{G}_E, \tag{9}$$

see the scheme in Fig. 2. The first part follows the Hooke's law to compute unregularized displacements $\mathbf{u}_f$ of image points. It says that the points move proportionally to the applied forces with a constant k. The filter $\mathbf{G}_I$ regularizes displacement improvements $\mathbf{u}_f$ and the second filter $\mathbf{G}_E$ regularizes the overall displacement field $\mathbf{u}$.

Fig. 2. The combined elastic-incremental model (Rogelj & Kovačič, 2004).

2.2.3 Local forces estimation and similarity measures

Local forces are obtained either by optimization or they are computed directly, depending on a particular registration method. In the former case, the registration is usually based on a global similarity measure which detects improvement of local image correspondence (Rueckert et al., 1999; Rohlfing et al., 2003), or block matching techniques are performed (Kostelec et al., 1998; Maintz et al., 1998). Most suitable translations are found in an optimization procedure with the use of monomodal as well as multimodal similarity measures. In the latter case, the forces are estimated in every point as the derivative of a similarity measure. The resulting dense field of the forces is used to compute a high dimensional deformation, often based on some physical interpretation. The registration methods which perform the high-dimensional warping are typically limited to monomodal data, e.g. (Gramkow & Bro-Nielsen, 1997; Christensen et al., 1996; Thirion, 1998). However, the effort to develop registration algorithms focused on high-dimensional matching of multimodal data recently emerged. In (Rogelj et al., 2003), point similarity measures are proposed for high dimensional deformable registration of multimodal data. The point similarity measures are derived from global similarity measures based on the joint PDF estimated from the joint histogram.

The point similarity measure $S_{MI}(\mathbf{x})$ derived from the global mutual information is defined as (Rogelj & Kovačič, 2003):

$$S_{MI}(\mathbf{x}) = \log_2 \frac{p_{MN}(m(\mathbf{x}), n(\mathbf{x}))}{p_M(m(\mathbf{x}))p_N(n(\mathbf{x}))} \tag{10}$$

The negative joint entropy $H(M,N)$, which is the most informative part of MI can be used as a global multimodal similarity measure and a point similarity measure S_H can be derived. In (Maintz et al., 1998), conditional probability densities are used for a region similarity measure, which is here rewritten as another point similarity measure:

$$S_{PC}(\mathbf{x}) = p\big(n(\mathbf{x}) \big| m(\mathbf{x})\big), \tag{11}$$

In (Rogelj et al., 2003), other measures are proposed:

$$S_U(\mathbf{x}) = \frac{p_{MN}(m(\mathbf{x}), n(\mathbf{x}))^2}{p_M(m(\mathbf{x}))p_N(n(\mathbf{x}))}, \tag{12}$$

$$S_{UH}(\mathbf{x}) = \log_2 p_{MN}(m(\mathbf{x}), n(\mathbf{x})) + \log_2 \frac{p_{MN}(m(\mathbf{x}), n(\mathbf{x}))}{p_M(m(\mathbf{x}))p_N(n(\mathbf{x}))} = S_H + S_{MI}\,. \tag{13}$$

There are measures expressed in the terms of probability (S_{PC}, S_U) and uncertainty (S_{MI}, S_H, S_{UH}). It was shown in the previous work (Schwarz et al., 2007) that better performance of the proposed registration methods is achieved involving the probability similarity measures and another point similarity measure depending on the probability was proposed there:

$$S_{PMI}(\mathbf{x}) = \frac{p_{MN}(m(\mathbf{x}), n(\mathbf{x}))}{p_M(m(\mathbf{x}))p_N(n(\mathbf{x}))}. \tag{14}$$

Any point similarity measure can be used to compute a region similarity measure by simply averaging the point similarities over the region. The averaging over a region can also be viewed as convolution filtering with some spatial filter (Rogelj & Kovačič, 2003). Convolution spatial filtering was previously described as a method for modeling spatial deformations. The regularization provided directly by region similarity measures is substantial for large regions. The concept of local forces based on the derivative of a point similarity measure is further extended in (Rogelj & Kovačič, 2003), where symmetric local forces are proposed to improve registration consistency.

3. Multimodal deformable registration in stereotaxic space

Two algorithms for atlas-based deformable registration of MRI brain images are proposed. The use of various multimodal similarity measures is explored. Their computation requires knowledge of the joint PDF of the images being registered. Its estimation is a common part in both algorithms. The algorithms differ in the other parts including extraction of local forces and spatial deformation models. The subjects' image data are supposed to be transformed into stereotaxic space by a previous linear registration step.

3.1 Low-dimensional deformable registration by enhanced block matching

The first registration algorithm produces low-dimensional deformations which are suitable for coarse spatial normalization which is an essential step in VBM. On the contrary to the widely used spatial normalization implemented in (Ashburner & Friston, 2000), the proposed algorithm is applicable for matching multimodal image data. It is in fact an enhanced block matching technique. The scheme of the algorithm is in Fig. 3. A multilevel subdivision is applied on a floating image N. Obtained rectangular image blocks are matched with a reference image M. The resulting displacement field $\mathbf{u}$ is made up from local translations of the image blocks by RBF interpolation. The translations representing warping forces $\mathbf{f}$ are found by maximizing symmetric regional similarity measures.

3.1.1 Symmetric regional matching

Conventional block matching techniques measure the similarity of the floating image regions with respect to the reference image. Here, inspired by the symmetric forces introduced for high dimensional matching (Rogelj & Kovačič, 2003), the regional similarity measure is computed by:

$$S_W^{sym} = S_W^{forward}\left[M(\mathbf{x}_W + \mathbf{u}_W(\mathbf{x}_W)), N(\mathbf{x}_W)\right] + S_W^{reverse}\left[M(\mathbf{x}_W), N(\mathbf{x}_W - \mathbf{u}_W(\mathbf{x}_W))\right], \tag{15}$$

where the first term corresponds to the similarity measure computed over all K_W voxels $\mathbf{x}_W=[\mathbf{x}_1, \mathbf{x}_2, ..., \mathbf{x}_{Kw}]$ of a region W of the floating image according to the reference image. The second term corresponds to the reverse direction. The terms $M(\mathbf{x}_W)$ and $N(\mathbf{x}_W)$ denotes all voxels of the region W in the reference image and in the floating image respectively. The displacements $\mathbf{u}_W(\mathbf{x}_W)=[\mathbf{u}(\mathbf{x}_1), \mathbf{u}(\mathbf{x}_2), ..., \mathbf{u}(\mathbf{x}_{Kw})]$ are computed in foregoing iterations and they moves the voxels $N(\mathbf{x}_W)$ of the floating image from their undeformed positions $\mathbf{x}_W$ to new positions $\mathbf{x}_W+\mathbf{u}_W(\mathbf{x}_W)$, where they get matched with the voxels $M(\mathbf{x}_W+\mathbf{u}_W(\mathbf{x}_W))$ of the reference image. In the case of the reverse similarity measure, the displacements $\mathbf{u}_W(\mathbf{x}_W)$ are applied on the reference image M, as it would be deformed by the inversion of the so far computed deformation. The voxels $M(\mathbf{x}_W)$ of the reference image are thus moved to get matched with the voxels $N(\mathbf{x}_W-\mathbf{u}_W(\mathbf{x}_W))$ of undeformed floating image, see the illustration in Fig. 4.

It is impossible to uniquely describe correspondences of regions in two images by multimodal similarity measures, due to their statistical character. When the local translations are searched in complex medical images, suboptimal solutions are obtained frequently with the use of the forward similarity measure only. Using the symmetric similarity measure, additional correspondence information is provided and the chance of getting trapped in local optima is thus reduced.

Due to the subvoxel accuracy of performed deformations, the point similarities have to be computed in points that are not positioned on the image grid. Point similarity functions (10)-(14) are defined for a finite number of intensity values due to histogram binning performed in the joint histogram computation. Conventional interpolation of voxel intensities is therefore inapplicable, because the point similarity functions are not defined for new values which would arise. Thus, the GPV method, which was originally designed for computation of joint intensity histogram, is used here. The computation of point pair similarity requires knowledge of the intensities m and n in the points of the images M and N respectively. The intensity n on a grid point of the deformed grid of the floating image is straight-forward, whereas the intensity m on a point off the regular grid of the reference

image is unknown. Their similarity is computed as a linear combination of similarities of intensity pairs corresponding to the points in the neighbour-hood of the examined point.

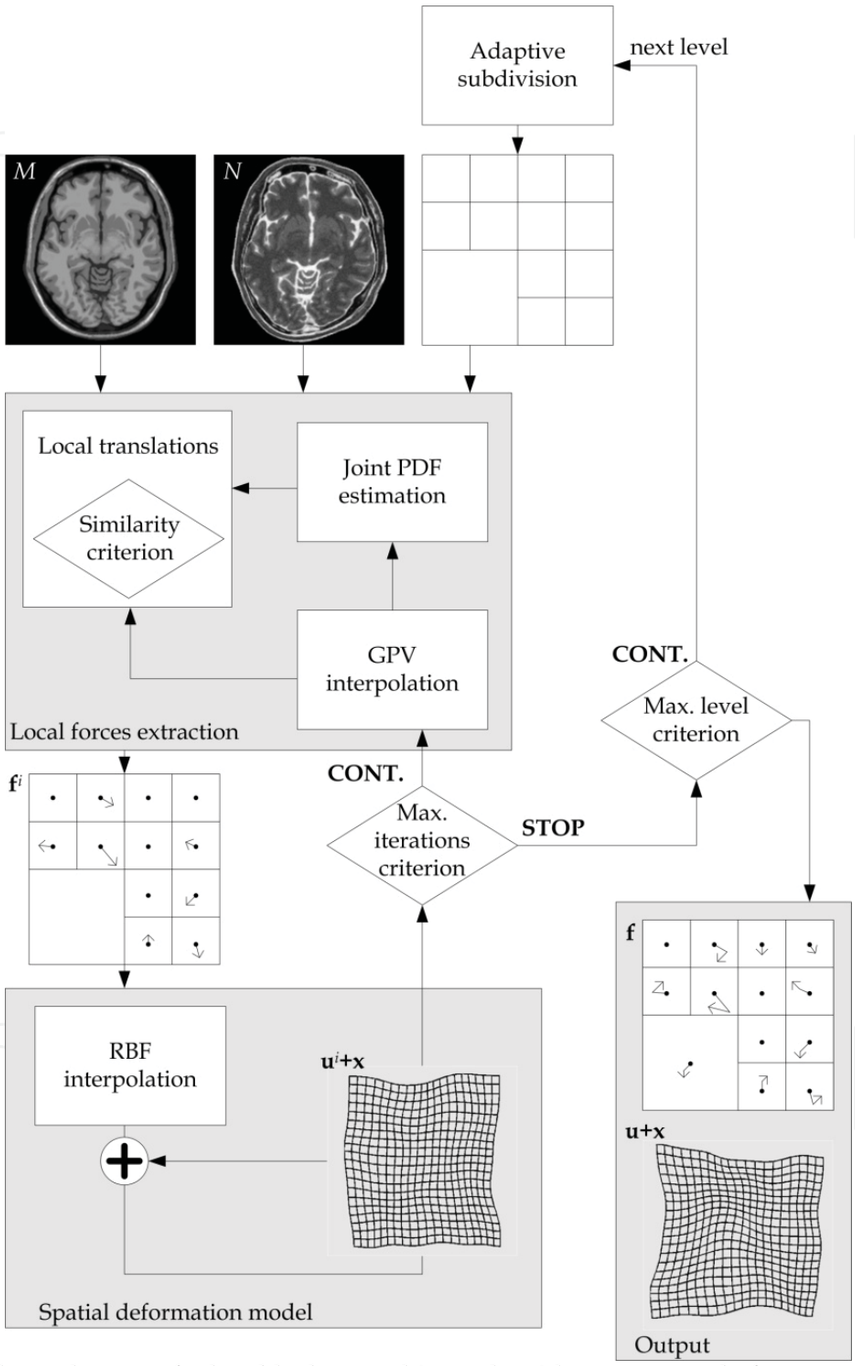

Fig. 3. The scheme of the block matching algorithm proposed for coarse spatial normalization.

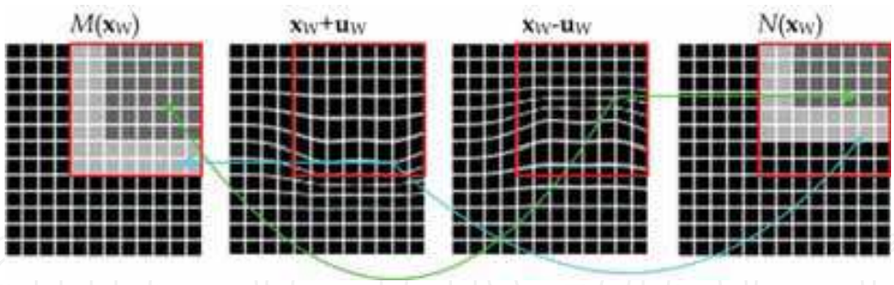

Fig. 4. Illustration of regional symmetric matching. The similarity is measured in the forward (the blue line) as well as in the reverse (the green line) direction of registration. In the forward direction, the displacement field computed so far is applied on the floating image voxels. In the reverse direction, the inverse displacement field is applied on the reference image voxels.

The extent of the neighbourhood depends on the chosen kernel function. Here, the first-order, the second-order and the third-order B-spline functions with 8, 27 and 64 grid points in neighbourhood for 3-D tasks or 4, 9 and 16 points in neighbourhood for 2-D tasks are used. The particular choice of the kernel function affects the smoothness of the behaviour of the regional similarity measure, see Fig. 5. The number of local optima is the lowest in the case of the third-order B-spline. As the evaluation of the B-splines increases the computational load, their values are computed only once and stored in a lookup table with increments equal to 0.001.

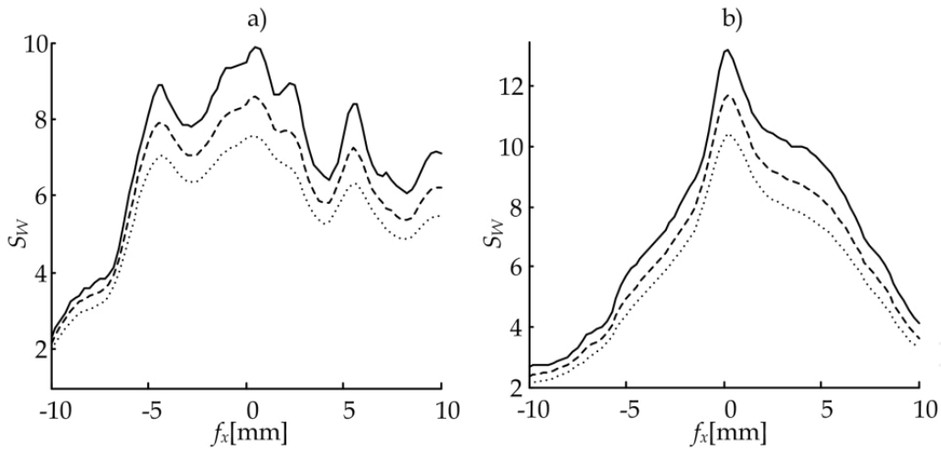

Fig. 5. Comparison of the regional similarity measure computed with the use of GPV and the first-order B-spline (solid line), the second-order B-spline (dashed line) and the third-order B-spline (dotted line). A region of the size a) 10x10 mm, b) 20x20 mm was translated by f_x=±10mm in the x direction.

Local translations which maximize a matching criterion are searched in optimization procedures. Here, the symmetric regional similarity measure is used as the matching criterion which has to be maximized:

$$S_W(\mathbf{f}_W) = S_W^{forward}\left(M(\mathbf{x}_W + \mathbf{u}_W(\mathbf{x}_W) + \mathbf{f}_W), N(\mathbf{x}_W)\right) + \\ + S_W^{reverse}\left(M(\mathbf{x}_W), N(\mathbf{x}_W - \mathbf{u}_W(\mathbf{x}_W) - \mathbf{f}_W)\right), \tag{16}$$

where $\mathbf{f}_W = [\mathbf{f}_1, \mathbf{f}_2, ..., \mathbf{f}_{Kw}]$, $\mathbf{f}_1 = \mathbf{f}_2 = ... \mathbf{f}_{Kw} = [f_x, f_y, f_z]^T$ is a translation of all voxels in a region W along x, y and z axis. The use of the symmetric regional similarity measure and the GPV interpolation with the use of the second-order B spline or the third order B-spline leads to well-behaved criterion function in the case of large regions. In the case of small regions, the uncertainty about the best translation is still high and many local maxima occur near the optimal solution. A combination of extensive search and hillclimbing algorithms is used here to find the global maximum. First, a space of all possible translations is determined by absolute maximum translation $|\mathbf{f}_{max}|$ in all directions. Then, the space of all possible translations is searched with a relatively big step s_e. The q best points are then used as starting points for the following hillclimbing with a finer step s_h. The maximum of q local maxima obtained by the hillclimbing is then declared as the global maximum, see Fig. 6. All the parameters of the optimization procedure depend on the size of the region which is translated. In this way, fewer criterion evaluations are done for larger regions when the chance of getting trapped into local maxima is reduced and more evaluations of the criterion is performed for smaller regions.

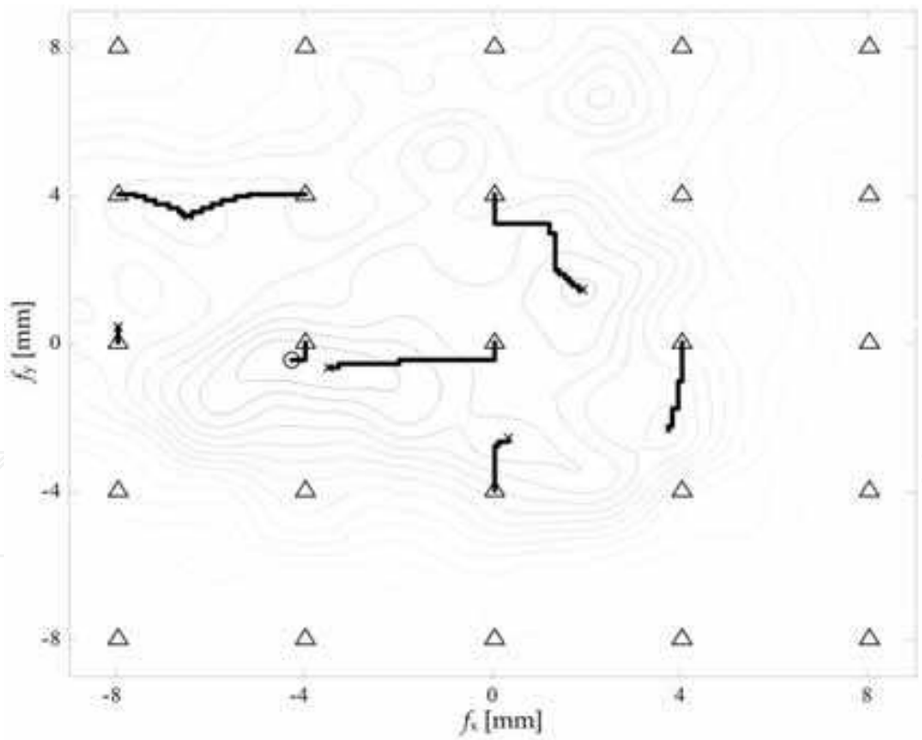

Fig. 6. A trajectory of 2-D optimization performed by an extensive search (triangles) combined with hillclimbing (bold lines). The optimization procedure was set for this illustration as follows: $|f_{max}| = [8, 8]$, $s_e = 4$ mm, $s_h = 0.1$ mm, $q = 8$. The local maxima are marked by crosses and the global one is marked by the circle.

Image deformation based on interpolation with the use of RBFs is used here. The control points $\mathbf{p}_i$ are placed into the centers of the regions and their translations $\mathbf{f}_i$ are obtained by symmetric regional matching. Substituting the translations into (6), three systems of linear equations are obtained and three vectors of w coefficients, where w is the number of the regions, $\mathbf{a}_k=(a_{1,k}, \ldots, a_{w,k})^T$ computed. The displacement of any point $\mathbf{x}$ is then defined separately for each dimension by the interpolant:

$$u_k(\mathbf{x}) = \sum_{i=1}^{w} a_{i,k} \psi_{CP}\left(\left\|\mathbf{x} - \mathbf{p}_i\right\|\right), \quad k = 1...3. \tag{17}$$

The values of spatial support s for various regions sizes are set empirically.
Optimal matches can be hardly found in a single pass composed of the local translations estimation and the RBF-based interpolation, since features in one location influence decisions at other locations of the images. Iterative updating scheme is therefore proposed here. A multilevel strategy is incorporated into the proposed algorithm. The deformation is iteratively refined in the coarse to fine manner. The size of the regions cannot be arbitrarily small, because the local translations are determined independently for each region and voxel interdependecies are introduced only by the regional similarity measure. The regions containing poor contour or surface information can be eliminated from the matching process and the algorithm can be accelerated in this way. The subdivision is performed only if at least one voxel in the current region has its normalized gradient image intensity bigger then a certain threshold.

3.2 High-dimensional deformable registration with the use of point similarity measures and wavelet smoothing

The second registration algorithm produces high dimensional deformations involving gross shape differences as well as local subtle differences between a subject and a template anatomy. As multimodal similarity measures are used, the algorithm is suitable for DBM on image data with different contrasts. There are two main parts repeated in an iterative process as it was in the block matching algorithm: extraction of local forces $\mathbf{f}$ by measurements of similarity and a spatial deformation model producing the displacement field $\mathbf{u}$. The main difference is that these parts are completely independent here, whereas the regional similarity measure used in the block matching technique constrains the deformation and thus it acts as a part of the spatial deformation model. Another difference is in the way of extraction of the local forces. No local optimization is done here and the forces are directly computed from the point similarity measures.
The registration algorithm is based on previous work and it differs from the one presented in (Schwarz et al., 2007) namely in the spatial deformation model. The scheme of the algorithm is in Fig. 7. The displacement field $\mathbf{u}$ which maximizes global mutual information between a reference image and a floating image is searched in an iterative process which involves computation of local forces $\mathbf{f}$ in each individual voxel $\mathbf{x}$ and their regularization by the spatial deformation model. The regularization has two steps here. First, the displacements proportional to forces are smoothed by wavelet thresholding. These displacements are integrated into final deformation, which is done iteratively by summation. The second part of the model represents behaviour of elastic materials where

displacements wane if the forces are retracted. This is ensured by the overall Gaussian smoother.

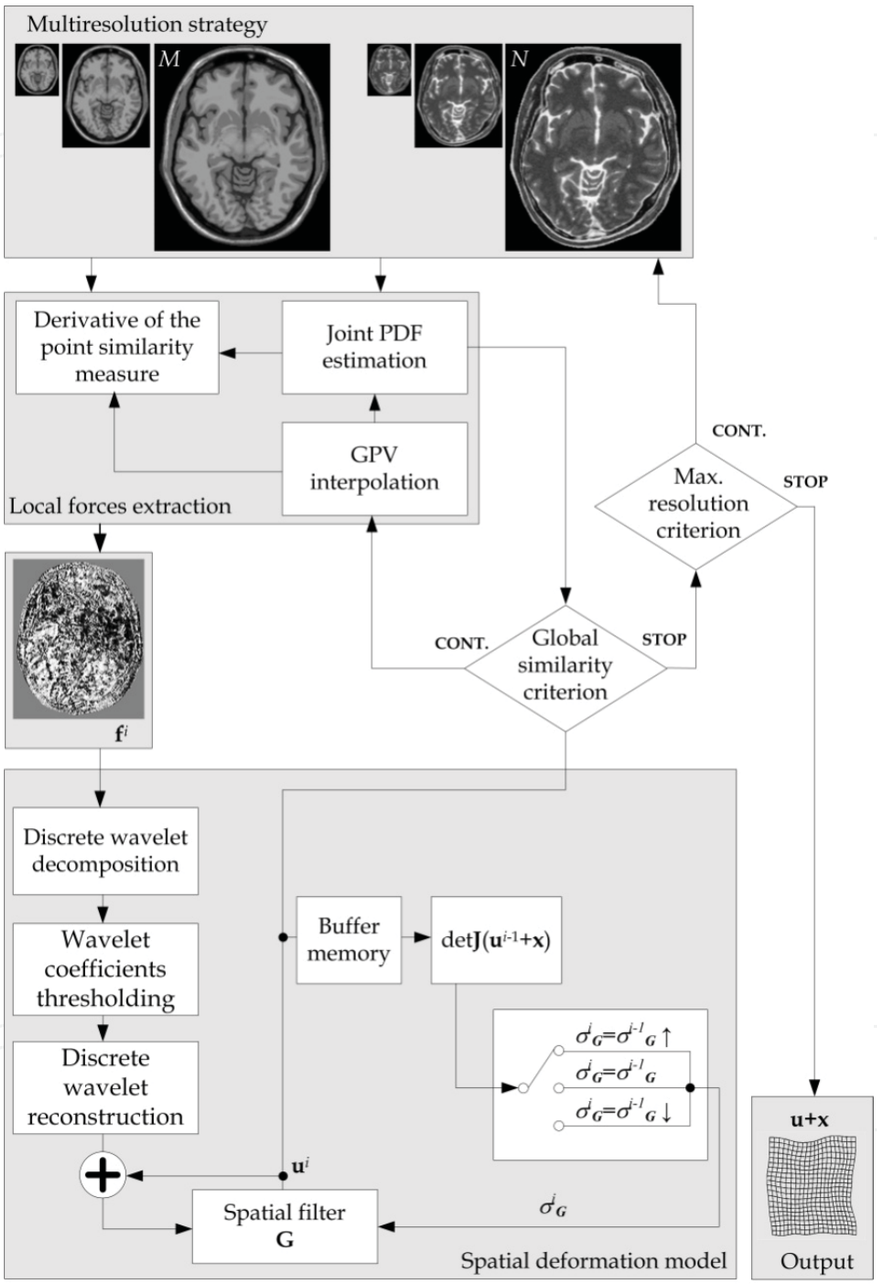

Fig. 7. The scheme of the high-dimensional registration algorithm proposed for DBM. The spatial deformation model consists of two basic components. First, the dense force field is smoothed by wavelet thresholding and then the displacements are regularized by Gaussian filtering to prevent breaking the topological condition of diffeomorphicity.

Nearly symmetric orthogonal wavelet bases (Abdelnour & Selesnick, 2001) are used for the decomposition and the reconstruction, which are performed in three levels here. All detail coefficients in the first and in the second level of decomposition are set to zero in the thresholding step of the algorithm. The initial setup of the standard deviation σ_G of the Gaussian filter is supposed to be found experimentally. The deformation has to preserve the topology, i.e. one-to-one mappings termed as diffeomorphic should only be produced. This requirement is satisfied if the determinant of the Jacobian of the deformation is held above zero:

$$\det \mathbf{J}(\varphi) \geq 0, \qquad \mathbf{J}(\varphi) = \begin{pmatrix} \frac{\partial \varphi_1}{\partial x} & \frac{\partial \varphi_1}{\partial y} & \frac{\partial \varphi_1}{\partial z} \\ \frac{\partial \varphi_2}{\partial x} & \frac{\partial \varphi_2}{\partial y} & \frac{\partial \varphi_2}{\partial z} \\ \frac{\partial \varphi_3}{\partial x} & \frac{\partial \varphi_3}{\partial y} & \frac{\partial \varphi_3}{\partial z} \end{pmatrix}. \tag{18}$$

where φ_1, φ_2 and φ_3 are components of the deformation over x, y and z axes respectively. The values of the Jacobian determinant are estimated by symmetric finite differences. The image is undesirably folded in the positions, where the Jacobian determinant is negative. In such a case, the deformation is not invertible. The σ_G-control block therefore ensures increments in σ_G if the minimum Jacobian determinant drops below a predefined threshold. On the other hand, the deformation should capture subtle anatomical variations among studied images. The σ_G-control block therefore ensures decrements in σ_G if the minimum Jacobian determinant starts growing during the registration process.

Local forces are computed for each voxel independently as the difference between forward forces and reverse forces, using the same symmetric registration approach as in the previously described block-matching technique. The forces are estimated by the gradient of a point similarity measure. The derivatives are approximated by central differences, such that the k^{th} component of a force at a voxel $\mathbf{x}$ is defined here as:

$$\begin{aligned} f_k(\mathbf{x}) &= f_k^{forward}(\mathbf{x}) - f_k^{reverse}(\mathbf{x}) = \\ &= \frac{S\left(M(\mathbf{x}+\mathbf{u}(\mathbf{x})+\varepsilon_k), N(\mathbf{x})\right) - S\left(M(\mathbf{x}+\mathbf{u}(\mathbf{x})-\varepsilon_k), N(\mathbf{x})\right)}{2\varepsilon_k} - \\ &- \frac{S\left(M(\mathbf{x}), N(\mathbf{x}-\mathbf{u}(\mathbf{x})+\varepsilon_k)\right) - S\left(M(\mathbf{x}), N(\mathbf{x}-\mathbf{u}(\mathbf{x})-\varepsilon_k)\right)}{2\varepsilon_k}, \quad k = 1 \ldots D, \end{aligned} \tag{19}$$

where ε_k is a voxel size component. The point similarity measure is evaluated in non-grid positions due to the displacement field applied on the image grids. Thus, GPV interpolation from neighboring grid points is employed here. For more details on computation and normalization of the local forces see (Schwarz et al., 2007).

3.3 Evaluation of deformable registration methods

The quality of the presented registration algorithms is assessed here on recovering synthetic deformations. The synthetic deformations based on thin-plate spline simulator (TPSsim) and Rogelj's spatial deformation simulator (RGsim) were applied to 2-D realistic T2-weighted MRI images with 3% noise and 20% intensity nonuniformity from the Simulated Brain Database (SBD) (Collins et al., 1998). The deformation simulators are described in detail in (Schwarz et al., 2007). The deformed images were then registered to artifact-free T1-weighted images from SBD and the error between the resulting and the initial deformation was measured. The appropriate evaluation measures are the root mean-squared residual displacement and the maximum absolute residual displacement. In the ideal case, the composition of the resulting and initial deformation should give an identity transform with no residual displacements.

Based on preliminary results and previous related works, the similarity measure S_{PMI} was used for both registration algorithms and the maximum level of subdivision in the block matching technique was set to 5. This level corresponds to the subimage size of 7x7 pixels. Although the next level of subdivision gave an increase in the global mutual information, the alignment expressed by quantitative evaluation measures and also by visual inspection was constant or worse.

The results expressed by root mean squared error displacements are presented in Table 1 and Table 2. The high-dimensional deformable registration technique gives more precise deformations with the respect to the lower residual error. The obtained results showed its ability to recover the smooth deformations generated by TPSsim as well as the complex deformations generated by RGsim.

$\lvert e_0^{MAX} \rvert$ [mm]	e_0^{RMS} [mm]	e^{RMS} [mm]											
		o_1	o_2	o_1	o_2	o_1	o_2	o_1	o_2	o_1	o_2	o_1	o_2
		1	1	2	1	3	1	2	2	3	2	3	3
TPSsim													
5	2.47	0.59	0.57	0.56	**0.51**	0.52	**0.51**						
8	3.95	0.74	0.71	0.69	0.68	**0.67**	**0.67**						
10	4.93	0.91	0.89	0.86	0.85	**0.82**	**0.82**						
12	5.92	1.17	1.38	1.34	**1.16**	1.36	1.35						
RGsim													
5	2.30	0.93	0.87	0.85	0.79	0.77	**0.75**						
8	3.67	1.47	1.41	1.37	1.39	1.33	**1.27**						
10	4.59	2.19	2.17	2.09	2.05	2.07	**1.98**						
12	5.51	3.09	2.93	**2.92**	3.05	2.93	2.99						

Table 1. Root mean squared error displacements achieved by the multilevel block matching technique on various initial misregistration levels expressed by $\lvert e_0^{MAX} \rvert$ and e_0^{RMS} and with various setups in GPV interpolation kernel functions. The order of B-splines used in joint PDF estimate construction is signed as o_1 and the order of B-splines used in regional matching is signed as o_2.

$\lvert e_0^{MAX} \rvert$ [mm]	e_0^{RMS} [mm]	e^{RMS} [mm]				
		σ_G=2.0 mm	σ_G=2.5 mm	σ_G=3.0 mm	σ_G=3.5 mm	σ_G=4.0 mm
RGsim						
2.30	2.47	1.10	0.73	**0.69**	0.93	0.93
3.67	3.95	1.87	**1.07**	1.09	1.70	1.72
4.59	4.93	2.70	**1.46**	1.52	2.56	2.62
5.51	5.92	3.69	**2.02**	2.19	3.65	3.73
TPSsim						
2.47	2.30	0.84	0.60	**0.53**	0.61	0.58
3.95	3.67	1.26	0.74	**0.68**	1.00	0.96
4.93	4.59	1.77	0.84	**0.78**	1.48	1.43
5.92	5.51	2.42	1.16	**0.98**	2.20	2.18

Table 2. Root mean squared error displacements achieved by the highdimensional deformable registration method on various initial misregistration levels expressed by $\lvert e_0^{MAX} \rvert$ and e_0^{RMS} and with various setups in σ_G . Highlighted values show the best results achieved with the registration algorithm.

4. Deformation-based morphometry on real MRI datasets

In this section the results of high-resolution DBM in the first-episode and chronic schizophrenia are presented, in order to demonstrate the ability of the high-dimensional registration technique to capture the complex pattern of brain pathology in this condition. High-resolution T1-weighted MRI brain scans of 192 male subjects were obtained with a Siemens 1.5 T system in Faculty Hospital Brno. The group contained 49 male subjects with first-episode schizophrenia (FES), 19 chronic schizophrenia subjects (CH) and 124 healthy controls. The template from SBD which is based on 27 scans of one subject was used as the reference anatomy and 192 template-to-subject registrations with the use of the presented high-dimensional technique were performed. The resulting displacement vector fields were converted into scalar fields by calculating Jacobian determinants in each voxel of the stereotaxic space. The scalar fields were put into statistical analysis which included assessing normality, parametric significance testing. The Jacobian determinant can be viewed as a parameter which characterizes local volume changes, i.e. local shrinkage or enlargement caused by a deformation. The analysis of the scalar fields produced spatial map of t statistic which allowed to localize regions with significant differences in volumes of anatomical structures between the groups. Complex patterns of brain anatomy changes in schizophrenia subjects as compared to healthy controls were detected, see Fig. 8.

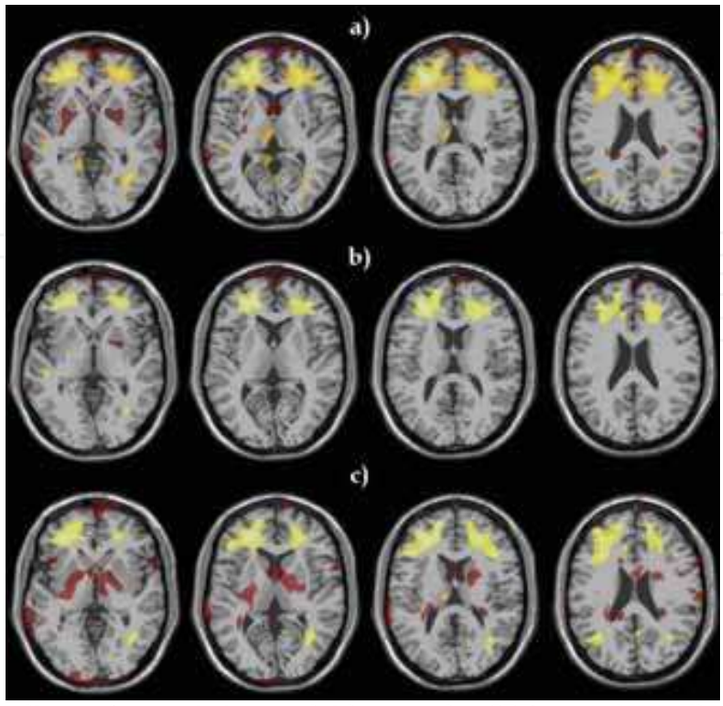

Fig. 8. Selected slices of t statistic overlaid over the SBD template. The t values were thresholded at the levels of significance α=5% corrected for multiple testing by the False Detection Rate method. The yellow regions represent local volume reductions in schizophrenia subjects compared to healthy controls and the red regions represent local volume enlargements. Compared groups: a) FES∪CH vs. NC, b) FES vs. NC, c) CH vs. NC.

5. Conclusion

In this chapter two deformable registration methods were described: 1) a block matching technique based on parametric transformations with radial basis functions and 2) a high-dimensional registration technique with nonparametric deformation models based on spatial smoothing. The use of multimodal similarity measures was insisted. The multimodal character of the methods make them robust to tissue intensity variations which can be result of multimodality imaging as well as neuropsychological diseases or even normal aging.

One of the described algorithms was demonstrated in the field of computational neuroanatomy, particularly for fully automated spatial detection of anatomical abnormalities in first-episode and chronic schizophrenia based on 3-D MRI brain scans.

Acknowledgement

The work was supported by grants IGA MH CZ NR No. 9893-4 and No. 10347-3.

References

Abdelnour, A. F. & Selesnick, I. W. (2001). Nearly symmetric orthogonal wavelet bases. *Proc. IEEE Int. Conf. Acoust., Speech, Signal Processing (ICASSP)*, May 2001, IEEE, Salt Lake City

Ali, A. A.; Dale, A. M.; Badea, A. & Johnson, G. A. (2005). Automated segmentation of neuroanatomical structures in multispectral MR microscopy of the mouse brain. *NeuroImage*, Vol. 27, No. 2, 425–435, ISSN 1053-8119

Alterovitz, R.; Goldberg, K.; Kurhanewicz, J.; Pouliot, J. & Hsu, I. (2004). Image registration for prostate MR spectroscopy using biomechanical modeling and optimization of force and stiffness parameters. *Proceedings of 26th Annual International Conference of IEEE Engineering in Medicine and Biology Society*, 2004, pp. 1722–1725, ISBN 0-7803-8440-7, IEEE, San Francisco

Amidror, I. (2002). Scattered data interpolation methods for electronic imaging systems: a survey. *Journal of Electronic Imaging*, Vol. 11, No. 2, pp.157–176, ISSN 1017-9909

Ashburner, J. & Friston, K. J. (2000). Voxel-based morphometry – the methods. *NeuroImage*, Vol. 11, No. 6, 805–821, ISSN 1053-8119

Ashburner, J. (2007). A fast diffeomorphic image registration algorithm. *NeuroImage*, Vol. 38, No. 1, 95–113, ISSN 1053-8119

Chen, H. & Varshney, P. K. (2003). Mutual information-based CT-MR brain image registration using generalized partial volume point histogram estimation. *IEEE Transactions on Medical Imaging*, Vol. 22, No. 9, 1111–1119, ISSN 0278-0062

Christensen, G. E.; Rabbitt, R. D. & Miller M. I. (1996). Deformable templates using large deformation kinematics. *IEEE Transactions on Image Processing*, Vol. 5, No. 10, 1435–1447, ISSN 0278-0062.

Clatz, O. et al. (2005). Robust nonrigid registration to capture brain shift from intraoperative MRI. *IEEE Transactions on Medical Imaging*, Vol. 24, No. 11, 1417–1427, ISSN 0278-0062.

Collins, D. L. et al. (1998). Design and construction of a realistic digital brain phantom.*IEEE Transactions on Medical Imaging*, Vol. 17, No. 3, 463–468, ISSN 0278-0062

Collins, D. L.; Neelin, P.; Peters, T. M. & Evans, A. C. (1994). Automatic 3D inter-subject registration of MR volumetric data in standardized Talairach space. *Journal of Computer Assisted Tomography*, Vol. 18, No. 2, 192–205, ISSN 0363-8715.

Čapek, M.; Mroz, L. & Wegenkittl, R. (2001). Robust and fast medical registration of 3D-multi-modality data sets. *Proceedings of the International Federation for Medical & Biological Engineering*, pp. 515–518, ISBN 953-184-023-7, Pula

Donato, G. & Belongie, S. (2002). Approximation methods for thin plate spline mappings and principal warps. *Proceedings of European Conference on Computer Vision*, pp. 531–542

Downie, T. R. & Silverman, B. W. (2001). A wavelet mixture approach to the estimation of image deformation functions. *Sankhya: The Indian Journal Of Statistics Series B*, Vol. 63, No. 2, 181–198, ISSN 0581-5738

Ferrant, M.; Warfield, S. K.; Nabavi, A.; Jolesz, F. A. & Kikinis, R. (2001). Registration of 3D intraoperative MR images of the brain using a finite element biomechanical model. In: *IEEE Transactions on Medical Imaging*, Vol. 20, No. 12, 1384–97, ISSN 0278-0062

Fornefett, M.; Rohr, K. & Stiehl, H. S. (2001). Radial basis functions with compact support for elastic registration of medical images. *Image and Vision Computing*, Vol. 19, No. 1, 87–96, ISSN 0262-8856

Friston, K. J. et al. (2007). *Statistical Parametric Mapping: The Analysis of Functional Brain Images*, Elsevier, ISBN 0123725607, London

Gaser, C. et al. (2001). Deformation-based morphometry and its relation to conventional volumetry of brain lateral ventricles in MRI. *NeuroImage*, Vol. 13, No. 6, 1140–1145, ISSN 1053-8119

Gaser, C. et al. (2004). Ventricular enlargement in schizophrenia related to volume reduction of the thalamus, striatum, and superior temporal cortex. *American Journal of Psychiatry*, Vol. 161, No. 1, 154–156, ISSN 0002-953X

Gholipour, A. et al. (2007). Brain functional localization: a survey of image registration techniques. *IEEE Transactions on Medical Imaging*, Vol. 26, No. 4, 427–451, ISSN 0278-0062.

Gramkow, C. & Bro-Nielsen, M. (1997). Comparison of three filters in the solution of the Navier-Stokes equation in registration. *Proceedings of Scandinavian Conference on Image Analysis SCIA'97*, 1997, pp. 795–802, Lappeenranta

Ibanez, L.; Schroeder, W.; Ng, L. & Cates, J. (2003). *The ITK Software Guide*. Kitware Inc, ISBN 1930934106

Kostelec, P.; Weaver, J. & Healy D. Jr. (1998). Multiresolution elastic image registration. *Medical Physics*, Vol. 25, No. 9, 1593–1604, ISSN 0094-2405

Kubečka, L. & Jan, J. (2004). Registration of bimodal retinal images - improving modifications. *Proceedings of 26th Annual International Conference of IEEE Engineering in Medicine and Biology Society*, pp. 1695–1698, ISBN 0-7803-8440-7, IEEE, San Francisco

Maes, F. (1998). Segmentation and registration of multimodal medical images: from theory, implementation and validation to a useful tool in clinical practice. Catholic University, Leuven

Maintz, J. B. A. & Viergever, M. A. (1998). A survey of medical image registration. *Medical Image Analysis*, Vol. 2, No. 1, 1–37, ISSN 1361-8415

Maintz, J. B. A.; Meijering, E. H. W. & Viergever, M. A. (1998). General multimodal elastic registration based on mutual Information. In: *Medical Imaging 1998: Image Processing*, Kenneth, M. & Hanson, (Ed.), 144–154, SPIE

Mechelli, A., Price, C. J., Friston, K. J. & Ashburner, J. (2005). Voxel-based morphometry of the human brain: methods and applications. *Current Medical Imaging Reviews*, vol. 1, No. 2, 105–113, ISSN 1573-4056

Modersitzki, J. (2004). *Numerical Methods for Image Registration*. Oxford University Press, ISBN 0198528418, New York.

Pauchard, Y.; Smith, M. R. & Mintchev, M. P. (2004). Modeling susceptibility difference artifacts produced by metallic implants in magnetic resonance imaging with point-based thin-plate spline image registration. *Proceedings of 26th Annual International Conference of IEEE Engineering in Medicine and Biology Society*, pp. 1766–1769, ISBN 0-7803-8440-7, IEEE, San Francisco

Peckar, W.; Schnörr, C.; Rohr, K.; Stiehl, H. S. & Spetzger, U. (1998). Linear and incremental estimation of elastic deformations in medical registration using prescribed displacements. *Machine Graphics & Vision*, Vol. 7, No. 4, 807–829, ISSN 1230-0535

Pluim, P. W. J.; Maintz J. B. A. & Viergever M. A. (2001). Mutual information matching in multiresolution contexts. *Image and Vision Computing*, Vol. 19, No. 1, 45–52, ISSN 0262-8856

Rogelj, P.; Kovačič, S. & Gee, J. C. (2003). Point similarity measures for non-rigid registration of multi-modal data. *Computer Vision and Image Understanding*, Vol. 92, No. 1, 112–140, ISSN 1077-3142

Rogelj, P. & Kovačič, S. (2003). Point similarity measure based on mutual information. In: *Biomedical Image Registration: Revised Papers*, Gee, J. C.; Maintz, J. B. A. & Vannier, M. W. (Ed.), 112–121, Springer-Verlag, ISBN 978-3-540-20343-8

Rogelj, P. & Kovačič, S. (2003). Symmetric image registration. *Medical Image Analysis*, Vol. 10, No. 3, 484–493, ISSN 1361-8415

Rogelj, P. & Kovačič, S. (2004). Spatial deformation models for non-rigid image registration. *Proceedings of 9th Computer Vision Winter Workshop CVWW'04*, 2004, pp. 79–88, Slovenian Pattern Recognition Society, Piran.

Rohlfing, T.; Maurer, C. R.; Bluemke, D. A. & Jacobs, M. A. (2003). Volume-preserving nonrigid registration of MR breast images using free-form deformation with an incompresibility constraint. *IEEE Transactions on Medical Imaging*, Vol. 12, No. 6, 730–741, ISSN 0278-0062.

Rohr, K. (2001). Elastic registration of multimodal medical images: a survey. *Künstliche Intelligenz*, Vol. 14, No. 3, 11–17, ISSN 0933-1875

Rueckert, D. et al. (1999). Nonrigid registration using free-form deformations: application to breast MR images. *IEEE Transactions on Medical Imaging*, Vol. 18, No. 8, 712–721, ISSN 0278-0062

Schnabel, J. A. et al. (2003). Validation of non-rigid image registration using finite element methods: application to breast MR images. *IEEE Transactions on Medical Imaging*, Vol. 22, No. 2, 238–247, ISSN 0278-0062.

Schwarz, D.; Kašpárek, T., Provazník, I. & Jarkovský, J. (2007). A deformable registration method for automated morphometry of MRI brain images in neuropsychiatric research. *IEEE Transactions on Medical Imaging*, Vol. 26, No. 4, 452-461, ISSN 0278-0062.

Studholme, C.; Hill, D. L. G.; & Hawkes, D. J. (1999). An overlap invariant entropy measure of 3D medical image alignment. *Pattern Recognition*, Vol. 32, No. 1, 71–86, ISSN 1054-6618

Thirion, J. P. (1998). Image matching as a diffusion process: an analogy with Maxwell's demons. *Medical Image Analysis*, Vol. 2, No. 3, 243–260, ISSN 1361-8415

Viola, P. & Wells, W. M. (1995). Alignment by maximization of mutual information. *International Journal of Computer Vision*, Vol. 24, No. 2, 137–154, ISSN 0920-5691

Wendland, H. (1995). Piecewise polynomial, positive definite and compactly supported radial functions of minimal degree. *Advances in Computational Mathematics*, Vol. 4, No. 1, 389–396, ISSN 1019-7168

Xu, L.; Groth, K. M.; Pearlson, G.; Schretlen, D. J.; Calhoun, V. D. (2008). Source-based morphometry: the use of independent component analysis to identify gray matter differences with application to schizophrenia. *Human Brain Mapping*, Vol. 30, No. 3, 711–724, ISSN 1065-9471

Zitova, B. and Flusser J. (2003). Image registration methods: a survey. *Image and Vision Computing*, Vol. 21, No. 11, 977–1000, ISSN 0262-8856

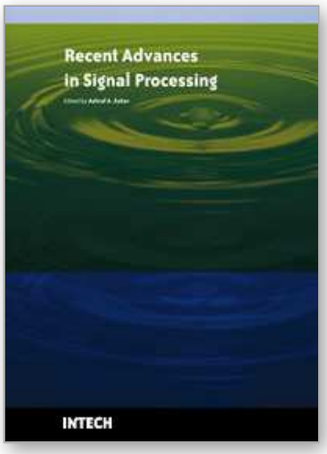

Recent Advances in Signal Processing

Edited by Ashraf A Zaher

ISBN 978-953-307-002-5

Hard cover, 544 pages

Publisher InTech

Published online 01, November, 2009

Published in print edition November, 2009

The signal processing task is a very critical issue in the majority of new technological inventions and challenges in a variety of applications in both science and engineering fields. Classical signal processing techniques have largely worked with mathematical models that are linear, local, stationary, and Gaussian. They have always favored closed-form tractability over real-world accuracy. These constraints were imposed by the lack of powerful computing tools. During the last few decades, signal processing theories, developments, and applications have matured rapidly and now include tools from many areas of mathematics, computer science, physics, and engineering. This book is targeted primarily toward both students and researchers who want to be exposed to a wide variety of signal processing techniques and algorithms. It includes 27 chapters that can be categorized into five different areas depending on the application at hand. These five categories are ordered to address image processing, speech processing, communication systems, time-series analysis, and educational packages respectively. The book has the advantage of providing a collection of applications that are completely independent and self-contained; thus, the interested reader can choose any chapter and skip to another without losing continuity.

InTech Europe
University Campus STeP Ri
Slavka Krautzeka 83/A
51000 Rijeka, Croatia
Phone: +385 (51) 770 447
Fax: +385 (51) 686 166
www.intechopen.com

InTech China
Unit 405, Office Block, Hotel Equatorial Shanghai
No.65, Yan An Road (West), Shanghai, 200040, China
中国上海市延安西路65号上海国际贵都大饭店办公楼405单元
Phone: +86-21-62489820
Fax: +86-21-62489821

IntechOpen